



High performance photomultiplication perovskite photodetectors with PC₆₀BM and NPB as the interlayers



Yue Fu ^{a,b}, Qiaogang Song ^{a,b}, Tong Lin ^{a,b}, Ye Wang ^{a,b}, Xue Sun ^{a,b}, Zisheng Su ^{a,*}, Bei Chu ^a, Fangming Jin ^a, Haifeng Zhao ^a, Wenlian Li ^a, C.S. Lee ^c

^a State Key Laboratory of Luminescence and Applications, Changchun Institute of Optics, Fine Mechanics, and Physics, Chinese Academy of Sciences, Changchun, 130033, People's Republic of China

^b University of Chinese Academy of Sciences, Beijing, 100039, People's Republic of China

^c Center of Super-Diamond and Advanced Films (COSDAF), Department of Physics and Materials Sciences, City University of Hong Kong, Hong Kong Special Administrative Region

ARTICLE INFO

Article history:

Received 1 July 2017

Received in revised form

14 September 2017

Accepted 14 September 2017

Available online 18 September 2017

Keywords:

Perovskite

Photodetectors

Dark current

Detectivity

ABSTRACT

Organic-inorganic hybrid perovskites have attracted more attention as successful light harvesting materials for solution-processed semiconductors and exhibit remarkable optoelectronic properties. Here photomultiplication-type photodetectors based on perovskite CH₃NH₃PbI₃ are demonstrated. By introducing suitable interlayers at the CH₃NH₃PbI₃/electrode interfaces, the performance of the photodetector is significantly improved. The optimized device with a *N,N*-di(naphthalene-1-yl)-*N,N*'-diphenylbenzidine anode interface layer and [6,6]-phenyl-C₆₀-butyric acidmethyl ester cathode interface layer shows a broadband response with a high photocurrent gain of about 177 and a high detectivity of 4.6 × 10¹³ Jones, which are higher than the reference device. Besides, the response speed of the device is also increased. The improvement is attributed to the improved charge carrier collection efficiency and suppressed dark current of the device.

© 2017 Elsevier B.V. All rights reserved.

1. Introduction

Photodetectors are the tools which can capture incident light and convert it into electronic signals, the light absorption material is thus critical for the devices. Recently, rapid progresses have been made in organic-inorganic perovskite solar cells [1–7], reaching a certified power conversion efficiency of 22.1% [8]. The organometal halide perovskite materials with layered structure present the properties of inorganic semiconductor materials and organic materials at the same time, and the cooperation of organic and inorganic components could greatly enhance the properties for each other. They do not only have the inorganic material properties of ultrafast charge generation, high mobility, and long charge carrier lifetime, but also enjoy the organic properties of easy fabrication and no deep-level defects. Semiconductor photodetectors with organic-inorganic halide perovskite materials which have high light absorption coefficients, large static dielectric constants (40–70) [9,10], high free carrier mobility [11], a partially tunable energy gap around 1.6 eV

[12,13], and long diffusion lengths [3,14–18] have many important applications in both industry and defense as well as scientific research [19–23]. Generally, there are typically two types of perovskite photodetectors, e.g., photodiode- and photomultiplication (PM)-types. For a photodiode-type photodetector, the external quantum efficiency (EQE) is generally lower than unity due to their limited light absorption efficiency, electron-hole pair (or exciton) dissociation efficiency, and charge-carrier collection efficiency [24–26]. On the other hand, the PM-type photodetector exhibits an EQE much higher than unity due to the mechanism that one incident photon can trigger more than one hole (or electron) flowing across the photodetector, indicating that a photocurrent gain of this device [27,28]. Due to their high responsivity and detectivity, PM-type perovskite photodetectors have drawn more and more attention recently [20,29]. Moehl. et al. observed a strong photocurrent amplification in a perovskite solar cell [30], and a direct contact of fluorine-doped tin oxide and perovskite is essential for the photocurrent amplification [31]. Dong et al. demonstrated a high photocurrent gain of about 500 in a perovskite photodetector by introducing a large concentration of Pb²⁺ cations in the top surface of the perovskite film [20]. Meanwhile, Liu et al. reported a perovskite

* Corresponding author.

E-mail address: suzs@ciomp.ac.cn (Z. Su).

photodetector with a photocurrent gain of about 45 through incorporating PbS quantum dots as the electron trap states [32]. Although high performance perovskite photodetectors have been demonstrated, their performance should be further improved for practical applications.

One of the factors that limit the performance of a photodetector is its dark current. The dark current can be controlled by the interface layer between the perovskite film and electrode. Thus appropriate choice of electrode interlayers is critical to improve the performance of perovskite photodetectors [21,26,33]. Besides, the charge carrier collection efficiency can also be modulated by the interface layers. Such a strategy has been demonstrated in photodiode-type perovskite photodetector [34]. However, it has never been exploited in PM-type counterparts. In this work, PM-type perovskite photodetectors based on $\text{CH}_3\text{NH}_3\text{PbI}_3$ (MAPbI_3) are fabricated, which shows a broad spectral response ranging from 300 to 800 nm. By adding N,N' -di(naphthalene-1-yl)- N,N' -diphenylbenzidine (NPB) and [6,6]-phenyl-C₆₀-butyric acidmethyl ester (PC₆₀BM) as the anode interface layer and cathode interface layer, respectively, the photodetector exhibits a low dark current and thus increased photocurrent gain of about 177 and detectivity of 4.6×10^{13} Jones at -1 V.

2. Experimental detail

Three photodetectors with the structures shown in Fig. 1a were fabricated:

- PD1: ITO/MAPbI₃/TAPC/MoO₃/Ag
- PD2: ITO/PC₆₀BM/MAPbI₃/TAPC/MoO₃/Ag
- PD3: ITO/PC₆₀BM/MAPbI₃/NPB/MoO₃/Ag

Here ITO is the cathode, PC₆₀BM is the cathode interface layer, MAPbI₃ is the active layer, the NPB or di-[4-(N,N-ditolyl-amino)-phenyl]cyclohexan (TAPC) is the anode interface layer, MoO₃ is used for anode modification, and Ag is the anode. The MAPbI₃ layers were prepared by a two steps spin-coating method similar to the literature [20]. PbI₂ was dissolved in anhydrous N,N -dimethylformamide to give a concentration of 600 mg/ml and the $\text{CH}_3\text{NH}_3\text{I}$ (MAI) was dissolved in 2-propanol to obtain a concentration of 43 mg/ml. ITO coated glasses were ultrasonically cleaned with acetone, ethanol, and deionized water for 15 min, respectively, and then treated with ultraviolet-ozone for 15 min before

fabrication of the photodetectors. PC₆₀BM with a concentration of 10 mg/ml dissolved in chlorobenzene solution was coated on ITO glass at 2000 rpm for 30 s, which formed a layer of about 80 nm. Then the PbI₂ solution was spun on ITO substrate at 3000 rpm for 60 s and dried at 70 °C for 5 min. The MAI solution was spun on top of dried PbI₂ film at 3000 rpm for 60 s and then annealed at 100 °C for 1 h, which formed MAPbI_3 layers with different thicknesses depended on the substrates. The device fabrication processes above were done in a nitrogen filled glovebox (<0.1 ppm H₂O and O₂). Subsequently, TAPC or NPB film (6 nm), 12 nm MoO₃, and 100 nm Ag were thermally evaporated sequentially on the MAPbI_3 layers under a pressure of 5.0×10^{-4} Pa. The photoactive area of the devices is 6 mm² as defined by the cross-bar configuration of the 2 mm wide ITO electrode and the 3 mm wide Ag electrode. X-ray diffraction (XRD) patterns were collected on a Bruker D8 Focus diffractometer with a Cu K α radiation ($\lambda = 1.54056$ Å) operated at 40 kV and 40 mA. Scanning electron microscopy (SEM) images were measured on a Hitachi S4800. Absorption spectra of the films on ITO-coated glass substrates were recorded with a Shimadzu UV-3101PC spectrophotometer. EQE spectra were performed with a Stanford SR803 lock-in amplifier under monochromatic illumination at a chopping frequency of 130 Hz by a Stanford SR540 chopper. Current-voltage (J-V) curves of the devices in the dark and under illumination were measured with a Keithley 2400 sourcemeter.

3. Results and discussion

The morphologies of the MAPbI_3 films on ITO and ITO/PC₆₀BM are shown in Fig. 2a and b. The two MAPbI_3 films have almost the same dense, homogeneous, and smooth morphology, indicating that the PC₆₀BM layer has little effect on the morphology of MAPbI_3 films, and the average grain size is about 400 nm. On contrast, the two films exhibit different thicknesses, as shown in the cross-sectional SEM images in Fig. 2c and d. The thickness of MAPbI_3 film on ITO is about 550 nm, while the total thickness of PC₆₀BM and MAPbI_3 film is 520 nm. This indicates MAPbI_3 film on PC₆₀BM has a lower thickness, which is attributed to the different roughness and surface properties of ITO and PC₆₀BM.

The XRD patterns of the two films are depicted in Fig. 3. Similarly, the two films also exhibit the same XRD pattern with no obvious impurity, indicating that the PC₆₀BM film has no impact on

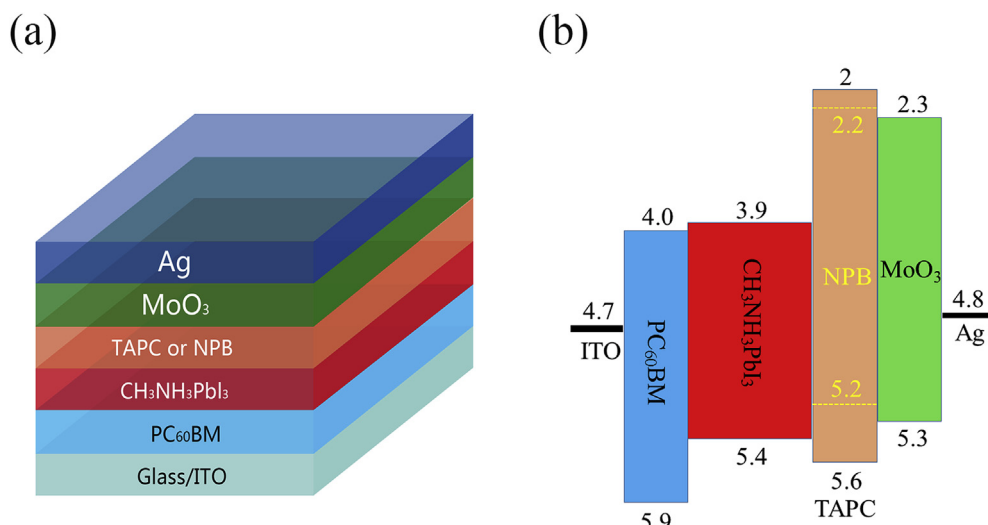


Fig. 1. (a) Device structure and (b) energy level diagram of the photodetectors.

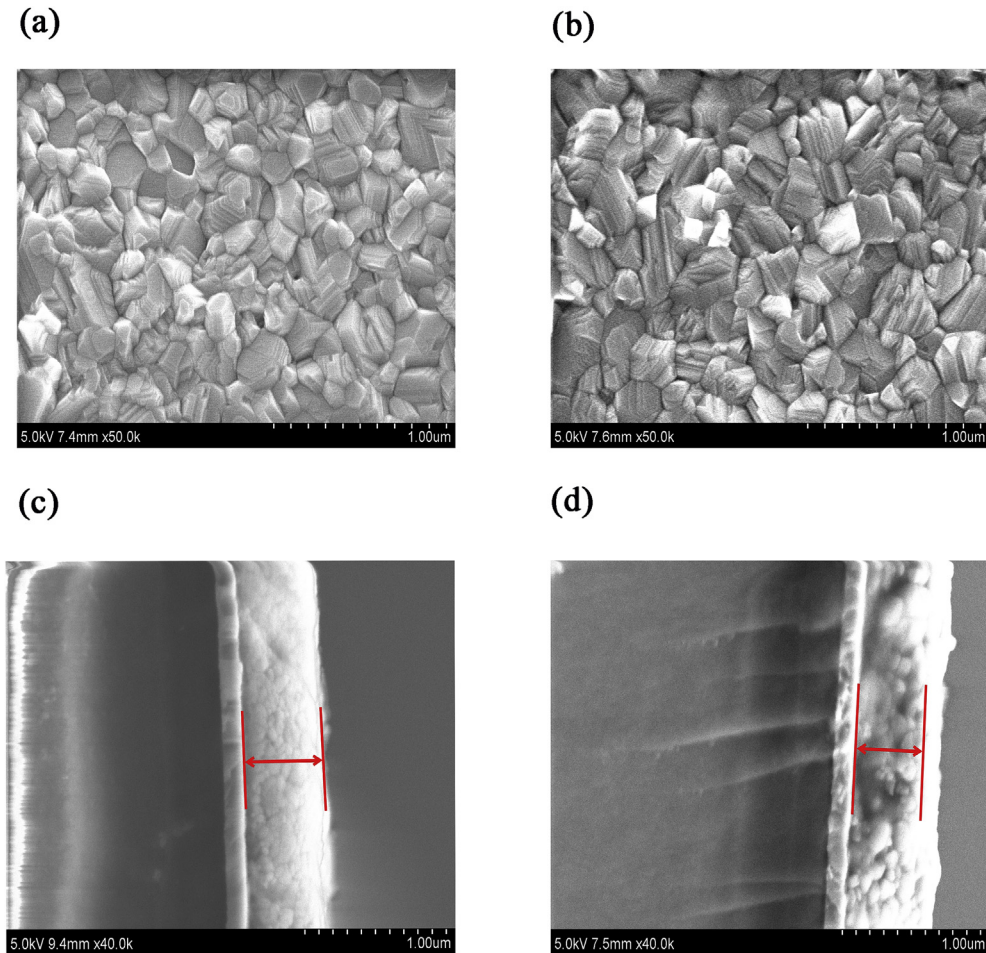


Fig. 2. SEM images of the surface of MAPbI₃ overlayers on the top of (a) ITO and (b) ITO/PC₆₀BM and Cross-sectional SEM images of the MAPbI₃ films on (c) ITO and (d) ITO/PC₆₀BM.

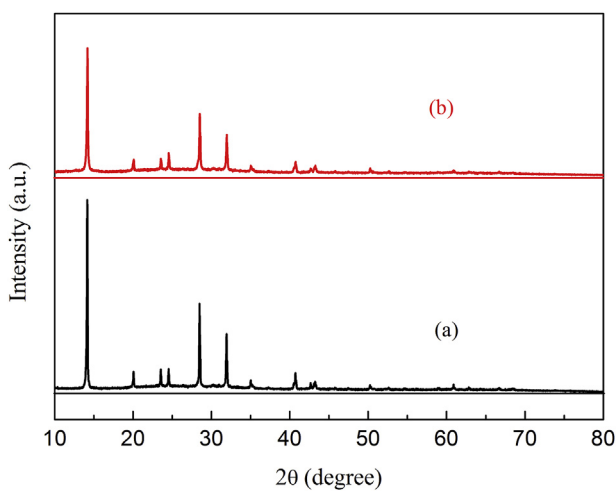


Fig. 3. XRD patterns of the MAPbI₃ films on (a) ITO and (b) ITO/PC₆₀BM.

the crystallizing of MAPbI₃ film. The diffraction peaks at 14.17°, 28.49°, and 43.27° can be assigned to the (110), (220), and (330) planes of MAPbI₃, respectively. The XRD patterns confirm a high degree of crystallinity and orientation of the MAPbI₃ films, which are similar to those reported for MAPbI₃ crystallized in the tetragonal perovskite structure with lattice parameters of

$a = b = 8.88 \text{ \AA}$ and $c = 12.68 \text{ \AA}$ [35–37].

The absorption spectra of the MAPbI₃ films on ITO and ITO/PC₆₀BM are displayed in Fig. 4, for reference, the absorption of PC₆₀BM is also provided. It can be found that PC₆₀BM primary absorb at shorter wavelength and MAPbI₃ films have a broad absorption band from 300 to 800 nm. However, the MAPbI₃ film on ITO has a little higher absorption at longer wavelength than that on

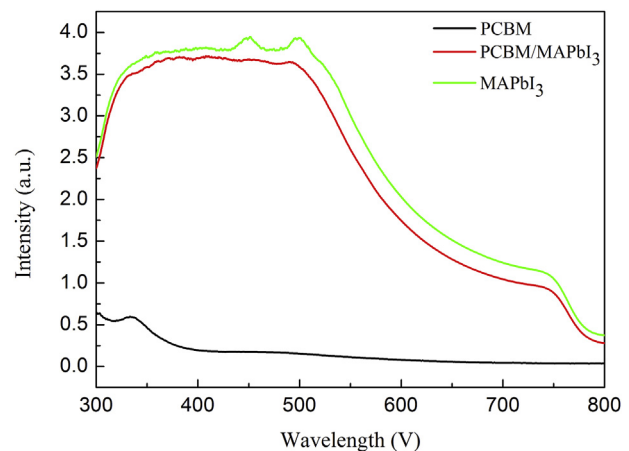


Fig. 4. Absorption spectra of PC₆₀BM and the MAPbI₃ films on ITO and ITO/PC₆₀BM.

ITO/PC₆₀BM, which is attributed to its higher thickness of the MAPbI₃ film. Meanwhile, the increased absorption of the PC₆₀BM/MAPbI₃ films at shorter wavelength is contributed to the absorption of PC₆₀BM.

Fig. 5 presents the dark current of the three photodetectors. Their dark currents are drastically different in the bias ranging from -1 to 1 V. Among the devices, PD1 shows the highest dark current in the negative voltage region. The dark current is decreased in PD2 with an additional PC₆₀BM layer, and it is further decreased when replacing TAPC with NPB. Meanwhile, PD3 has the highest dark current in the positive voltage region. As a result, PD3 exhibits the highest rectification ratio of about 100 at ± 1 V while it is only about 10 for both PD1 and PD2. MAPbI₃ is a bipolar transporting material [38], and the introduction of PC₆₀BM between ITO and MAPbI₃ effectively avoids the direct transport of holes to ITO electrode and suppress the leakage current. Besides, from the energy level diagram shown in Fig. 1b, the highest occupied molecular orbital (HOMO) level of PC₆₀BM is lower than that of MAPbI₃, resulting in a lower dark current of PD2 and PD3 in negative voltage region. On the other hand, MoO₃ can form a charge transfer complex with NPB, increasing the number of holes in the HTL [39]. Besides, the HOMO level of NPB is lower than TAPC. These effects result in a lower hole injection or extraction barriers and hence a higher dark current of PD3 at positive voltage region. These results indicate that the dark current of perovskite photodetectors can be efficiently suppressed by incorporating suitable interface buffer layers. Evidently, the dark current of a photodetector should be as low as possible to increase weak optical signal detection ability.

The spectral responsivity (R) indicates how efficient the detector responds to an optical signal and it is defined as the ratio of the photocurrent to the incident light intensity:

$$R = \frac{J_{ph}}{L_{light}} \quad (1)$$

where J_{ph} is the photocurrent and L_{light} is the incident light intensity. Fig. 6a plots the responsivity of the photodetectors at zero bias. As can be seen from the figure, all the three photodetectors present a broad response in the visible region, which is nearly consistent with the absorption spectrum of MAPbI₃. Besides, the three photodetectors reveal almost the same sharp response spectrum, indicating that the absorptions of the interlayers have no contribution to the photocurrent of the devices. On the other hand, the responsivity of PD2 with an additional PC₆₀BM layer is higher than PD1 in the whole response region, and the responsivity is

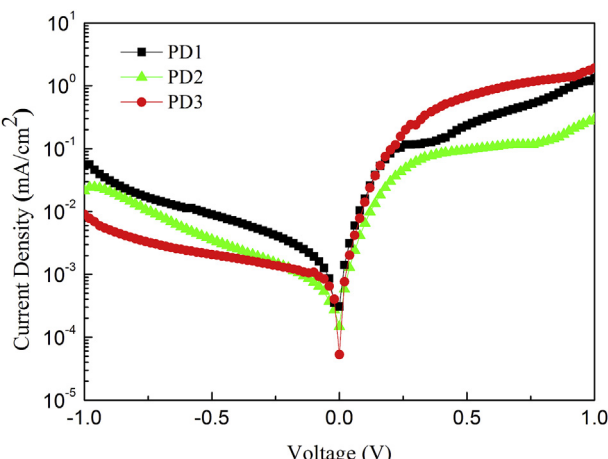


Fig. 5. Dark current of the photodetectors.

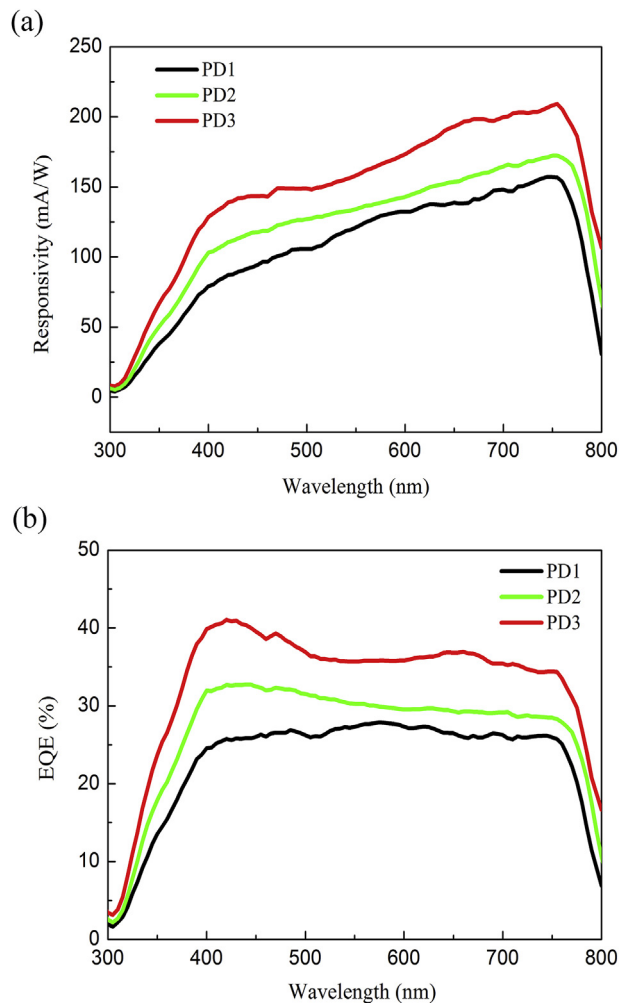


Fig. 6. (a) Spectral responsivity and (b) EQE spectra of the photodetectors at zero bias.

further improved for PD3 by replacing TAPC with NPB. The maximum responsivity of PD1 is 157 mA/W at 745 nm, while it is 171 and 207 mA/W for PD2 and PD3, respectively. The EQE spectra of the three devices are shown in Fig. 6b. Correspondingly, PD3 has the highest EQE in the whole response region among the three devices. This increased response can be attributed to the improved excitation dissociation efficiency and charge carrier collection efficiency [40,41].

To evaluate their performance at higher negative voltage, photocurrents of the devices are measured under illumination of a 550 nm light with an intensity of 257 $\mu\text{W}/\text{cm}^2$. As expected, PD3 has the highest photocurrent at zero bias. The photocurrent of the devices increase fast at low voltage and then gradually increases with applied negative voltage, as shown in Fig. 7. A high photocurrent of 20.24 mA/cm² is observed for PD3 at -1 V, suggesting an ON/OFF current ratio in the orders of 10³ when compared with its dark current. Correspondingly, the EQEs also increase fast at low voltage and exceed 100% at a voltage lower than -0.1 V. An EQE higher than 100% indicates a photocurrent gain of the device. A highest EQE of $1.77 \times 10^4\%$ is found for PD3 at -1 V, corresponding to a photocurrent gain of 177, which is one of the highest values among the reported perovskite photodetectors [20,42,43]. As mentioned above, MoO₃ can form a charge transfer complex with NPB, increasing the number of holes in the HTL [39]. On the other hand, Pb²⁺ clusters are formed on the top of MAPbI₃ layers because

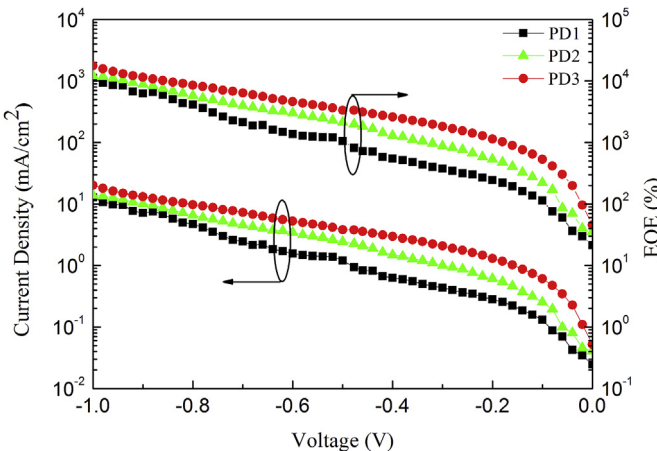


Fig. 7. The J-V curves and their EQE curves of the photodetectors under illumination of a 550 nm light with an intensity of 257 $\mu\text{W}/\text{cm}^2$.

a large amount of PbI_2 compared with MAI is used in preparing the films. The Pb^{2+} clusters will act as the traps for photogenerated holes [20]. These two effects result in hole trapped in the anode interface layers, which reduces electron injection barrier from Ag electrode under negative bias. Thus the amount of the injected charges can be significantly higher than the photogenerated ones, resulting in the photocurrent gain of the devices.

Fig. 8 shows the photocurrent as a function of illumination intensity of PD3 at 0 and -1 V, respectively. Here an AM1.5 solar simulator (Newport 94023A) is used as the illumination source and the intensity is varied from 0.06 to 75.7 mW/cm^2 . It can be found that a linear relationship is observed between the photocurrent and the light intensity both at 0 and -1 V. Such a linear response is important for a photodetector. However, at higher illumination density, the photocurrent deviates from this linear relationship, which should be attributed to the increased charge carrier recombination probability due to the higher density of the photo-generated charge carrier.

Detectivity (D^*) is another figure of merit factor of a photodetector and it can be given by: [2,26].

$$D^* = \frac{(Af)^{1/2}}{R/i_n} \quad (2)$$

where A is the effective area of the detector, f is the electrical bandwidth, and i_n is the noise current. When the dark current is

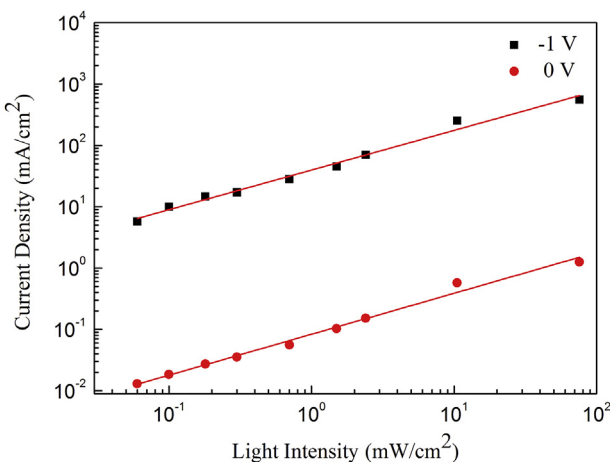


Fig. 8. Photocurrent as a function of illumination intensity of PD3 at different voltage.

dominated by the shot noise, D^* can be expressed as: [2,26].

$$D^* = \frac{R}{(2qJ_d)^{1/2}} \quad (3)$$

where q is the elementary electron charge and J_d is the dark current. All the three photodetectors exhibit a D^* in the order of 10^{12} Jones at 550 nm at -0.1 V. The D^* are 1.2×10^{12} , 1.9×10^{12} , and 4.3×10^{12} Jones for PD1, PD2, and PD3, respectively. The highest D^* of PD3 is attributed to its lower dark current and higher responsivity. While at -1 V, the D^* of three photodetectors are increased to 1.2×10^{13} , 2.1×10^{13} , and 4.6×10^{13} Jones, respectively, which are among the highest values for reported PM-type perovskite photodetectors [20,32,42,43]. The improved D^* at higher voltage are attributed to the higher photocurrent gain of the photodetectors.

To investigate the response speed of the photodetectors, their responses to a time-varying square wave white light (23.50 mW/cm^2) at 0 V are investigated, as shown in Fig. 9. The rise time and decay time are defined as the time taken for the initial current to increase to 90% of the peak value, or vice versa, respectively. It can be found that PD3 shows the highest response among the three devices, which is consistent with the EQE shows in Fig. 6. The rise time and decay of PD1 are 19.6 and 8.8 ms, while they are 19.5 and 7.1 ms for PD2 and 7.5 and 6.7 ms for PD3, respectively. The fast response speed of PD3 can be attributed to the higher charge carrier extraction efficiency [39]. The transient photocurrent response of PD3 was investigated by biasing the device at different voltages under the same light illumination (Fig. 10), and no obvious difference in the transient response is observed. This is different from that reported by Domanski et al. where a significant reduced response speed was found at higher negative voltage [42]. The difference should be attributed to the different photocurrent gain mechanisms of the devices, which is originated from the ion migration in the devices reported by Domanski et al. [42].

4. Conclusion

In summary, PM-type photodetectors composed of organic-inorganic perovskite MAPbI_3 are demonstrated. By introducing suitable interlayers at the MAPbI_3 /electrode interfaces, the performance of the photodetector is significantly improved. The optimized device shows a broadband response with a high photocurrent gain of about 177 and a high detectivity of 4.6×10^{13} Jones. Besides, the response speed is also increased. The

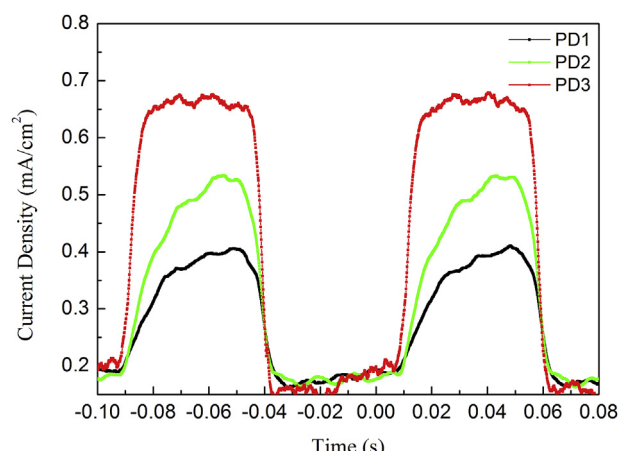


Fig. 9. Transient photocurrent curves of the photodetectors under illumination of a chopper modulated white light of 23.50 mW/cm^2 .

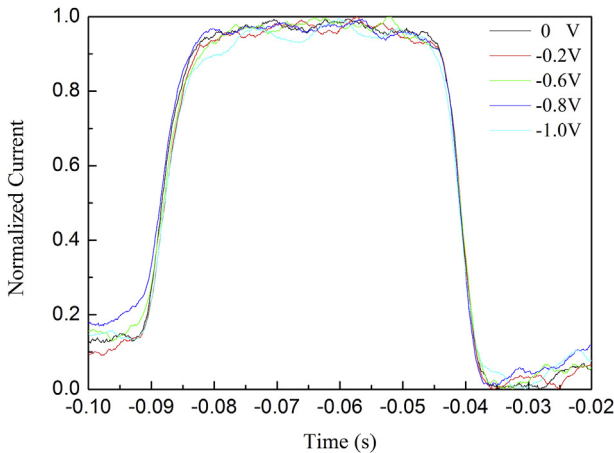


Fig. 10. Normalized transient photocurrent responses of PD3 under different bias.

improvement is attributed to the improved charge carrier collection efficiency. The excellent performance of this perovskite photodetector makes it potential in applications like communication, imaging, and defense.

Acknowledgements

This work was supported by the National Natural Science Foundation of China (61575192, 61604149, 61376062, and 61376022) and the project of Jiangsu Key Laboratory for Carbon-Based Functional Materials and Devices (KJS1615).

References

- [1] A. Kojima, K. Teshima, Y. Shirai, T. Miyasaka, Organometal halide perovskites as visible-light sensitizers for photovoltaic cells, *J. Am. Chem. Soc.* 131 (17) (2009) 6050–6051.
- [2] Fan Zuo, Spencer T. Williams, Po-Wei Liang, Chu-Chen Chueh, Chien-Yi Liao, Alex K.-Y. Jen, Binary-Metal perovskites toward high-performance planar-heterojunction hybrid solar cells, *Adv. Mater.* 26 (37) (2014) 6454–6460.
- [3] N.J. Jeon, J.H. Noh, W.S. Yang, Y.C. Kim, S. Ryu, J. Seo, S.I. Seok, Compositional engineering of perovskite materials for high-performance solar cells, *Nature* 517 (7535) (2015) 476–480.
- [4] J. You, L. Meng, T.B. Song, T.F. Guo, Y.M. Yang, W.H. Chang, Z. Hong, H. Chen, H. Zhou, Q. Chen, Y. Liu, N. De Marco, Y. Yang, Improved air stability of perovskite solar cells via solution-processed metal oxide transport layers, *Nat. Nanotechnol.* 11 (1) (2016) 75–81.
- [5] A. Mei, X. Li, L. Liu, Z. Ku, T. Liu, Y. Rong, M. Xu, M. Hu, J. Chen, Y. Yang, M. Grätzel, H. Han, A hole-conductor-free, fully printable mesoscopic perovskite solar cell with high stability, *Sci. (New York, N.Y.)* 345 (6194) (2014) 295–298.
- [6] M. Saliba, T. Matsui, K. Domanski, J.-Y. Seo, A. Ummadisingu, S.M. Zakeeruddin, J.-P. Correa-Baena, W.R. Tress, A. Abate, A. Hagfeldt, M. Grätzel, Incorporation of rubidium cations into perovskite solar cells improves photovoltaic performance, *Science* 354 (6309) (2016) 206–209.
- [7] F. Hou, Z. Su, F. Jin, X. Yan, L. Wang, H. Zhao, J. Zhu, B. Chu, W. Li, Efficient and stable planar heterojunction perovskite solar cells with an MoO₃/PEDOT: PSS hole transporting layer, *Nanoscale* 7 (2015) 9427–9432.
- [8] E. Zheng, B. Yuh, G.A. Tosado, Q. Yu, Solution-processed visible-blind UV-A photodetectors based on CH₃NH₃PbCl₃ perovskite thin films, *J. Mater. Chem. C* 5 (2017) 3796–3806.
- [9] Qianqian Lin, Ardalan Armin, Ravi Chandra Raju Nagiri, Paul L. Burn, Paul Meredith, Electro-optics of perovskite solar cells, *Nat. Photonics* 9 (2) (2014) 106–112.
- [10] J.M. Frost, K.T. Butler, F. Brivio, C.H. Hendon, M. van Schilfgaarde, A. Walsh, Atomistic origins of high-performance in hybrid halide perovskite solar cells, *Nano Lett.* 14 (5) (2014) 2584–2590.
- [11] Tomas Leijtens, Samuel D. Stranks, Giles E. Eperon, Rebecka Lindblad, Erik M.J. Johansson, Ian J. McPherson, Håkan Rensmo, James M. Ball, Michael M. Lee, Henry J. Snaith, Electronic properties of meso-superstructured and planar organometal halide perovskite films: charge trapping, photodoping, and carrier mobility, *ACS Nano* 8 (7) (2014) 7147–7155.
- [12] G. Xing, N. Mathews, S.S. Lim, N. Yantara, X. Liu, D. Sabba, M. Grätzel, S. Mhaisalkar, T.C. Sum, Low-temperature solution-processed wavelength-tunable perovskites for lasing, *Nat. Mater.* 13 (5) (2014) 476–480.
- [13] K.G. Lim, H.B. Kim, J. Jeong, H. Kim, J.Y. Kim, T.W. Lee, Boosting the power conversion efficiency of perovskite solar cells using self-organized polymeric hole extraction layers with high work function, *Adv. Mater.* 26 (2014) 6461–6466.
- [14] H. Zhou, Q. Chen, G. Li, S. Luo, T.B. Song, H.S. Duan, Z. Hong, J. You, Y. Liu, Y. Yang, Photovoltaics. Interface engineering of highly efficient perovskite solar cells, *Sci. (New York, N.Y.)* 345 (6196) (2014) 542–546.
- [15] Martin A. Green, Keith Emery, Yoshihiro Hishikawa, Wilhelm Warta, Ewan D. Dunlop, Solar cell efficiency tables (version 46), *Prog. Photovoltaics Res. Appl.* 23 (7) (2015) 805–812.
- [16] Michael Saliba, Taisuke Matsui, Ji-Youn Seo, Konrad Domanski, Juan-Pablo Correa-Baena, Mohammad Khaja Nazeeruddin, Shaik M. Zakeeruddin, Wolfgang Tress, Antonio Abate, Anders Hagfeldt, Michael Grätzel, Cesium-containing triple cation perovskite solar cells: improved stability, reproducibility and high efficiency, *Energy Environ. Sci.* 9 (6) (2016) 1989–1997.
- [17] Nakita K. Noel, Samuel D. Stranks, Antonio Abate, Christian Wehrenfennig, Simone Guarnera, Amir-Abbas Haghhighirad, Aditya Sadhanala, Giles E. Eperon, Sandeep K. Pathak, Michael B. Johnston, Annamaria Petrozza, Laura M. Herz, Henry J. Snaith, Lead-free organic–inorganic tin halide perovskites for photovoltaic applications, *Energy Environ. Sci.* 7 (9) (2014) 3061–3068.
- [18] Y.-C. Zhao, W.-K. Zhou, X. Zhou, K.-H. Liu, D.-P. Yu, Q. Zhao, Quantification of light-enhanced ionic transport in lead iodide perovskite thin films and its solar cell applications, *Light Sci. Appl.* 6 (2016), e16243.
- [19] L. Dou, Y.M. Yang, J. You, Z. Hong, W.H. Chang, G. Li, Y. Yang, Solution-processed hybrid perovskite photodetectors with high detectivity, *Nat. Commun.* 5 (2014) 5404.
- [20] R. Dong, Y. Fang, J. Chae, J. Dai, Z. Xiao, Q. Dong, Y. Yuan, A. Centrone, X.C. Zeng, J. Huang, High-gain and low-driving-voltage photodetectors based on organolead triiodide perovskites, *Adv. Mater. Deerf. Beach Fla.* 27 (11) (2015) 1912–1918.
- [21] B.R. Sutherland, A.K. Johnston, A.H. Ip, J. Xu, V. Adinolfi, P. Kanjanaboos, E.H. Sargent, Sensitive, fast, and stable perovskite photodetectors exploiting interface engineering, *Acs. Photonics* 2 (2015) 1117–1123.
- [22] X. Gong, M. Tong, Y. Xia, W. Cai, J.S. Moon, Y. Cao, G. Yu, C.L. Shieh, B. Nilsson, A.J. Heeger, High-detectivity polymer photodetectors with spectral response from 300 nm to 1450 nm, *Sci. (New York, N.Y.)* 325 (5948) (2009) 1665–1667.
- [23] G. Konstantatos, E.H. Sargent, Nanostructured materials for photon detection, *Nat. Nanotechnol.* 5 (6) (2010) 391–400.
- [24] Z. Su, F. Hou, X. Wang, Y. Gao, F. Jin, G. Zhang, Y. Li, L. Zhang, B. Chu, W. Li, High-performance organic small-molecule panchromatic photodetectors, *Acs. Appl. Mater. Interfaces* 7 (2015) 2529–2534.
- [25] Dezhai Yang, Xiaokang Zhou, Dongge Ma, Fast response organic photodetectors with high detectivity based on rubrene and C₆₀, *Org. Electron.* 14 (11) (2013) 3019–3023.
- [26] Q. Lin, A. Armin, D.M. Lyons, P.L. Burn, P. Meredith, Low noise, IR-blind organohalide perovskite photodiodes for visible light detection and imaging, *Adv. Mater. Deerf. Beach Fla.* 27 (12) (2015) 2060–2064.
- [27] F. Guo, B. Yang, Y. Yuan, Z. Xiao, Q. Dong, Y. Bi, J. Huang, A nanocomposite ultraviolet photodetector based on interfacial trap-controlled charge injection, *Nat. Nanotechnol.* 7 (12) (2012) 798–802.
- [28] R. Saran, V. Stolojan, R.J. Curry, Ultrahigh performance C₆₀ nanorod large area flexible photoconductor devices via ultralow organic and inorganic photo-doping, *Sci. Rep.* 4 (2014) 5041.
- [29] Yusheng Wang, Yupeng Zhang, Yao Lu, Weidong Xu, Haoran Mu, Caiyun Chen, Hong Qiao, Jingchao Song, Shaojuan Li, Baoquan Sun, Yi-Bing Cheng, Qiaoliang Bao, Hybrid graphene-perovskite phototransistors with ultrahigh responsivity and gain, *Adv. Opt. Mater.* 3 (10) (2015) 1389–1396.
- [30] T. Moehl, J.H. Im, Y.H. Lee, K. Domanski, F. Giordano, S.M. Zakeeruddin, M.I. Dar, L.-P. Heiniger, M.K. Nazeeruddin, N.-G. Park, M. Grätzel, Strong photocurrent amplification in perovskite solar cells with a porous TiO₂ blocking layer under reverse bias, *J. Phys. Chem. Lett.* 5 (2014) 3931–3936.
- [31] H.W. Chen, N. Sakai, A.K. Jena, Y. Sanehira, M. Ikegami, K.C. Ho, T. Miyasaka, A switchable high-sensitivity photodetecting and photovoltaic device with perovskite absorber, *J. Phys. Chem. Lett.* 6 (9) (2015) 1773–1779.
- [32] Chang Liu, Hui Peng, Kai Wang, Chunding Wei, Zixin Wang, Xiong Gong, PbS quantum dots-induced trap-assisted charge injection in perovskite photodetectors, *Nano Energy* 30 (2016) 27–35.
- [33] Y. Wang, D. Yang, X. Zhou, S.M. Alshehri, T. Ahamad, A. Vadim, D. Ma, CH₃NH₃PbI₃/C₆₀ heterojunction photodetectors with low dark current and high detectivity, *Org. Electron.* 42 (2017) 203–208.
- [34] Yanjun Fang, Jinsong Huang, Resolving Weak Light of Sub-picowatt per Square Centimeter by Hybrid Perovskite Photodetectors Enabled by Noise Reduction, *Adv. Mater.* 27 (17) (2015) 2804–2810.
- [35] L. Etgar, P. Gao, Z. Xue, Q. Peng, A.K. Chandiran, B. Liu, M.K. Nazeeruddin, M. Grätzel, Mesoscopic CH₃NH₃PbI₃/TiO₂ heterojunction solar cells, *J. Am. Chem. Soc.* 134 (2012) 17396–17399.
- [36] A. Kojima, K. Teshima, Y. Shirai, T. Miyasaka, Organometal halide perovskites as visible-light sensitizers for photovoltaic cells, *J. Am. Chem. Soc.* 131 (17) (2009) 6050–6051.
- [37] T. Baikie, Y. Fang, J.M. Kadro, M. Schreyer, F. Wei, S.G. Mhaisalkar, M. Graetzel, T.J. White, Synthesis and crystal chemistry of the hybrid perovskite (CH₃NH₃)PbI₃ for solid-state sensitised solar cell applications, *J. Mater. Chem. A* 1 (2013) 5628–5641.
- [38] Mingzhen Liu, Michael B. Johnston, Henry J. Snaith, Efficient planar heterojunction perovskite solar cells by vapour deposition, *Nature* 501 (7467) (2013)

- 395–398.
- [39] C.-I. Wu, C.-T. Lin, G.-R. Lee, T.-Y. Cho, C.-C. Wu, T.-W. Pi, Electronic and chemical properties of molybdenum oxide doped hole injection layers in organic light emitting diodes, *J. Appl. Phys.* 105 (2009), 033717.
- [40] S. Ryu, J. Seo, S.S. Shin, Y.C. Kim, N.J. Jeon, J.H. Noh, S.I. Seok, Fabrication of metal-oxide-free $\text{CH}_3\text{NH}_3\text{PbI}_3$ perovskite solar cells processed at low temperature, *J. Mater. Chem. A* 3 (2015) 3271–3275.
- [41] Jong H. Kim, Chu-Chen Chueh, Spencer T. Williams, Alex K.-Y. Jen, Room-temperature, solution-processable organic electron extraction layer for high-performance planar heterojunction perovskite solar cells, *Nanoscale* 7 (41) (2015) 17343–17349.
- [42] Konrad Domanski, Wolfgang Tress, Thomas Moehl, Michael Saliba, Mohammad Khaja Nazeeruddin, Michael Grätzel, Working principles of perovskite photodetectors: analyzing the interplay between photoconductivity and voltage-driven energy-level alignment, *Adv. Funct. Mater.* 25 (44) (2015) 6936–6947.
- [43] Y. Lee, J. Kwon, E. Hwang, C.H. Ra, W.J. Yoo, J.H. Ahn, J.H. Park, J.H. Cho, High-performance perovskite-graphene hybrid photodetector, *Adv. Mater. Deerf. Beach Fla.* 27 (1) (2015) 41–46.